Saudi Journal of Biological Sciences 29 (2022) 228–238

Contents lists available at ScienceDirect

Saudi Journal of Biological Sciences

journal homepage: www.sciencedirect.com

Original article

Green synthesis of Silver nanoparticles using *Streptomyces hirsutus* strain SNPGA-8 and their characterization, antimicrobial activity, and anticancer activity against human lung carcinoma cell line A549

Pallavi S.S. [a], Hassan Ahmed Rudayni [b], Asmatanzeem Bepari [c], Shaik Kalimulla Niazi [d], Sreenivasa Nayaka [a,*]

[a] Department of Studies in Botany, Karnatak University, Dharwad 580003, Karnataka, India
[b] Biology Department, College of Science, Al Imam Mohammad Ibn Saud Islamic University (IMSIU), Riyadh 11623, Saudi Arabia
[c] Department of Basic Health Sciences, College of Medicine, Princess Nourah bint Abdulrahman University, Riyadh 11671, Saudi Arabia
[d] Department of Preparatory Health Sciences, Riyadh Elm University, Riyadh 12611, Saudi Arabia

ARTICLE INFO

Article history:
Received 6 June 2021
Revised 16 August 2021
Accepted 23 August 2021
Available online 28 August 2021

Keyword:
Streptomyces
Silver nanoparticles
SDS-PAGE
Anticancer
A-549 cell line

ABSTRACT

The current study described the systematic and detailed extracellular synthesis method of silver nanoparticles (AgNPs) using *Streptomyces hirsutus* strain SNPGA-8 by green synthesis method. The AgNPs were subjected for characterizations using UV–Vis, FTIR, TGA, TEM, EDX, XRD, and zeta-potential analyses. The antibacterial activity against *Staphylococcus aureus*, *Pseudomonas aeruginosa*, *Enterococcus faecalis*, *Escherichia coli*, *Candida albicans*, *Alternaria alternata*, *Candida glabrata* and *Fusarium oxysporum* was determined by the agar well diffusion technique. The cytotoxicity of AgNPs against human lung cancer (A549) was studied by MTT and ROS assays and capping of proteins of AgNPs from SDS-PAGE. In the UV–Vis., absorption peak was found at 418 nm, FTIR analysis revealed the infrared bands of specific functional groups from 3273 cm^{-1} to 428 cm^{-1}; TEM data confirmed the spherical shape, smallest size of particle as 18.99 nm, while EDX analysis confirmed the elemental composition of AgNPs with 22.24% Ag. The XRD pattern confirmed the nature of AgNPs as crystalline, and zeta potential peak was found at −24.6 mV indicating the higher stability. The AgNPs exhibited increased antimicrobial activity with increase in dosage volume and considerable MIC and MBC values against microbial pathogens. In the MTT cytotoxicity assay, the IC_{50} value of 31.41 µg/mL is obtained against A549 cell line, suggesting the potential of AgNPs to inhibit the tumour cells; and ROS assay displayed increased ROS production with increase in treatment time. Based on the results, it is evident that *Streptomyces hirsutus* strain SNPGA-8 AgNPs are potentially promising to be applied for biomedical uses.

1. Introduction

Nanotechnology is one of the most vital research areas in material science that mainly deals with nanoparticle synthesis and applications. Metal nanoparticles possess unique physical traits like size, shape, and a larger surface area to volume ratio. The synthesis of nanoparticles is done from various metals like gold (Camas et al., 2019), silver (Nayaka et al., 2020a), copper (Hassan et al., 2019), magnesium (Imani & Safaei, 2019), zinc (Kalpana et al., 2018; Menazea & Awwad, 2020), and titanium (Eisa et al., 2020). However, AgNPs are gaining great interest due to their diversified utilization in various areas such as biosensing (Salem & Fouda, 2021), drug delivery (Lee & Jun 2019), nano-device fabrication, medicine (Ahmed & Mustafa, 2020; Zahin et al., 2020) gene delivery systems (Sung & Kim, 2019), and artificial implants (Ziąbka et al., 2018).

The biological synthesis of AgNPs provides advantages over physical and chemical synthesis methods as being eco-friendly, feasible, and easily scalable for extensive quantity synthesis. Among all the novel metals, silver has been used as an antimicrobial agent since ancient times. It has gained significant attention due to its medicinal, clinical, and culinary properties, with recently

* Corresponding author.
E-mail addresses: sreenivasanayaka06@gmail.com, sreenivasankud@gmail.com (S. Nayaka).
Peer review under responsibility of King Saud University.

Production and hosting by Elsevier

https://doi.org/10.1016/j.sjbs.2021.08.084
1319-562X/

observed enormous effectiveness as an anticancer agent (Tian et al., 2020; Wolny-Koładka & Malina, 2018)

Recently, many scientists have made efforts to make use of different microorganisms, including fungi, bacteria, yeast, and Actinomycetes, that can produce inorganic nanoparticles through either intracellular or extracellular routes. With recent progress and ongoing efforts to synthesize silver nanoparticles in biomedical uses, we selected Actinomycetes among the other microorganisms to synthesize AgNPs. Actinomycetes belong to the order *Actinomycetales*, which are characterized by spore formation, aerobic, gram-positive, distinguishable substrate, and aerial mycelia. The discovery of Actinomycetes potential to produce novel antibiotic and other therapeutically useful compounds through screening of secondary metabolites is becoming significantly important (Culp et al., 2019), like antitumor agents (Wypij et al., 2018), immunosuppressive (Manivasagan et al., 2014), and enzymes which are employed for industrial purposes (Ratnakomala et al., 2019). The bactericidal (Avilala & Golla, 2019), fungicidal (Vijayabharathi et al., 2018), antioxidant (Dholakiya et al., 2017), cytotoxic (Hamed et al., 2020), anti-algal (Zhang et al., 2015), anti-helminthic (Mikhailova, 2020), larvicidal (Dahari et al., 2016) and anti-inflammatory (Ma et al., 2018) activity play crucial role in the field of bio-pharmaceutics. Actinomycetes are considered efficient candidates for metal nanoparticle production either by extracellular or intracellular synthesis as they produce stable and polydispersed metal nanoparticles (Kumari et al., 2020).

Cancer cells exhibit uncontrolled cell division and cause noticeable mortality in both men and women and has been estimated to account for one-third of the sex disparity and other major health problems worldwide (Bray et al., 2018), so there is an urgent need for non-toxic, inexpensive, and effective treatments with minimal side effects. At present, silver nanoparticles has activity against several types of cancer cell lines, such as A549 (Saravanakumar et al., 2019), MCF-7 (Barai et al., 2018), and others.

The present study considers the potential of the Actinomycete isolate *Streptomyces hirsutus* strain SNPGA-8 for the green synthesis of AgNPs for the first time report and investigation of their antimicrobial activities against pathogenic bacteria, fungi including antitumor potential against human lung cancer (A549) cell lines with ROS expression (reactive oxygen species) level and isolation of extracellular capping proteins by SDS-PAGE.

2. Materials and methods

2.1. Isolation of Actinomycetes strains

Total 45 Actinomycetes strains with different colony morphologies were isolated using sediment samples collected from different locations of Maravanthe beach (Latitude 13°43′28.0″N and longitude 74°38′23.3″E), Kundapura, Udupi district, Karnataka, India. The collected samples were kept inside the dryer for one week to reduce the population of unwanted bacteria. About 0.2 mL suspension was taken from each tube of serially diluted (10^{-1} to 10^{-5}) sample and inoculated on the starch casein agar (SCA) media and incubated at 30 °C to 33 °C for seven days. The microbial contamination was avoided using fluconazole and streptomycin as antifungal and antibiotic, respectively and pure cultures of Actinomycetes were isolated by following the streak plate technique. A potent single Actinomycete was selected for the green synthesis of AgNPs and labelled as strain SNPGA-8.

2.2. Preparation of cell-free extract

For the preparation of Actinomycetes broth inoculum, a loop full of spores of strain SNPGA-8 was transferred into 50 mL of starch casein broth in a conical flask. For AgNPs production, SNPGA-8 inoculum was prepared in a 250 mL conical flask containing SC broth and was kept for incubation on a rotary shaker at 150 rpm for five days at 33 °C. After the incubation period, the culture was subjected to centrifugation at 5500 rpm (REMI R-24) to collect the supernatant required to synthesize AgNPs.

2.3. Green synthesis of AgNPs

One mM aqueous silver nitrate ($AgNO_3$) solution was mixed with cell-free supernatant in equal volumes and pH was adjusted at 8.5, and the mixture was stored in dark chamber for 120 hr for incubation. The silver ion reduction was examined by the colour change in the solution, which turned from pale yellow to dark-brown colour at the end of the incubation period.

2.4. Characterizations of AgNPs

2.4.1. UV–Visible (UV–Vis.) spectrophotometer

The synthesis of AgNPs was confirmed by the peak observed in UV–Vis. graph of the reaction mixture, when scanned between 300 and 700 nm with UV–Visible double beam spectrophotometer (METASHUV-9000A).

2.4.2. Fourier transform infrared spectroscopy (FTIR)

The AgNPs dried particle to prepare the pellet by mixing it with potassium bromide (KBr) and studied for the presence of IR bands. The scanning data obtained in the range of 4000 to 400 cm^{-1} with 4 cm^{-1} resolution to determine the functional groups present in the sample using the FTIR instrument (Nicolet 6700, Thermo Fisher Scientific).

2.4.3. TGA (Thermo gravimetric) analysis

The thermal behavior of the synthesized AgNPs with respect to their weight and temperature, the TGA is performed. In the TGA technique, the weight is measured as it is heated and cooled. Initially, the weight of the AgNPs is measured by analytical balance, and then the sample is placed inside the furnace. Gradually the temperature will be increased by passing inert gas over it, and corresponding to that, the weight of the sample is measured. Due to chemical reactions and combustion, there may be a loss in the weight of the sample. Thermo gravimetric analysis was carried out with a heating rate of 10 °C/min from room temperature to 600 °C using a TA instrument (SDT Q 600 and DSC Q20 USA).

2.4.4. Scanning electron microscope (SEM) with energy dispersive X-ray (EDX) analysis

The oven-dried AgNPs were loaded onto the stub with carbon tape fixed and coated by sputtering with gold. The prepared sample was investigated to determine the morphology of AgNPs and characteristics of elemental analysis of AgNPs with the help of SEM equipped with EDX (JEOL, JSM-IT 500LA).

2.4.5. High-resolution transmission electron microscope (HR-TEM) analysis

The morphological details, including the shape and size of the biosynthesized AgNPs were by HR-TEM analysis. The sample preparation for TEM was prepared by loading a drop of synthesized AgNPs suspension on a grid of copper coated with carbon and dried using a vacuum desiccator. The surface morphology of synthesized AgNPs was observed using Image J 1.45s software (FEI, TECNAI G2, F30).

2.4.6. X-ray diffraction (XRD) analysis

Fine powdered AgNPs were taken and mounted on a quartz glass slide to make a thin film and later were scanned with 2θ

angles from 20 to 80°at 40 kV and 30 mA to determine the crystalline structure and size of the particle (Rigaku, Smart-Lab SE). Measurement of particle size of AgNPs by using the Debye-Scherer equation ($D = (k\ \lambda)/\beta\ \cos\theta$), where, D = Crystalline size, k = constant, λ = X-ray wavelength, β = Full width half maximum, and cosθ = observed peak angle.

2.4.7. Zeta potential analysis

The prepared AgNPs solution was centrifuged for 20 min at 8000 rpm to collect supernatant and diluted with distilled water, followed by ultrasonication for 15 min. Then the zeta potential was analyzed through HORIBA, zeta analyzer instrument.

2.5. Genotypic characterization of a potent isolate

The isolated strain SNPGA-8 was employed to extract genomic DNA following the standard instructions of the Hi-Pura DNA purification kit. The 16S rRNA gene was sequenced (Sanger sequencing 3500 series, Genetic analyzer) and deposited to the NCBI database via nucleotide BLAST (BLASTn) web portal. Similar DNA sequences were selected to construct a phylogenetic tree using MegAlign Pro 17 (DNASTAR Lasergene) software as per the standard procedure.

2.6. Antimicrobial activity of AgNPs

The antimicrobial activity of AgNPs was performed by employing the agar well diffusion method against four bacterial pathogens, namely *Staphylococcus aureus* (MTCC6908), *Pseudomonas aeruginosa* (MTCC424), *Enterococcus faecalis* (MTCC6845), and *Escherichia coli* (MTCC40). For antifungal activity, *Candida albicans* (MTCC227), *Alternaria alternata* (MTCC2060), *Candida glabrata* (MTCC3814), and *Fusarium oxysporum* (MTCC2087), were used as test pathogens. The suspension of AgNPs at concentration of 1 mg/mL was prepared by suspending 10 mg of synthesized AgNPs in 10 mL distilled water and used as stock solution for further studies. The bacterial and fungal cultures were spread on Mueller- Hinton agar plate using sterile cotton swabs, and 6 mm wells were made with a cork borer and loaded with AgNPs of different volumes (25, 50, 75, and 100 μL). A 50 μL of sterile distilled water was poured as a negative control, streptomycin (25 μg/mL) and fluconazole (25 μg/mL) were used as standard (positive control) After 24 hr incubation at 33 °C, the radius around each well was taken as an inhibition zone and measured in mm.

2.7. Minimum inhibitory concentration (MIC) and minimum bactericidal concentration (MBC)

The MIC and MBC of biosynthesized AgNPs were carried out according to the method described (Nayaka et al., 2020b). The MIC was performed through broth dilution assay in 96 well microtiter plate using resazurin to determine the minimum concentration of nanoparticles required to inhibit pathogenic bacterial growth, whereas; the MBC was carried out on Mueller-Hinton agar plates. For MIC, the concentration of the bacterial inoculum was acclimated to 106 Mcfarland standards. 100 μL of AgNPs from 500 μg/mL of stock solution was diluted two folds with Muller-Hinton broth containing bacterial inoculums from column 12 to column 3 of the microtiter plate. Column 1 (only medium) and column 2 (medium with bacterial inoculum) served as negative and positive controls. The highest concentration of AgNPs was contained in column 12, whereas; the lowest concentration was contained in column 3. Later, 30 μL of resazurin solution was added to each well, and the plates were incubated at 37 °C for 24 hr. The MIC value of AgNPs was calculated after 24 hr of incubation. The MBC test was accomplished by spreading the suspension taken from each well of the microtiter plate onto Muller-Hinton agar plates. The plates were incubated at 37 °C for 48 hr, and the concentration where no bacterial growth was observed on plate was taken as MBC value.

2.8. Anticancer activity by cell viability (MTT) assay

The cytotoxic effect of synthesized AgNPs against the A549 cell line was determined using MTT assay (# 4060 Himedia) as previously described (Cory et al., 1991). The A549 cell lines were obtained from NCCS (National Centre for Cell Science) Pune, India. The cells were culture in Dulbecco modified eagle medium (DMEM-High Glucose (#AL111, Himedia), supplemented with 10% Fetal bovine serum (#RM10432, Himedia) in tissue culture flasks, and incubated in a CO_2 incubator with 5% CO_2 and humidified atmosphere at 37 °C for 24 hr. After incubation, the cells were carefully treated with trypsin and counted; further, cells were (20,000 cells/well in 200 μL of medium) placed into 96 well plates. An AgNPs suspension prepared in dimethyl sulfoxide (DMSO, # PHR1309, Sigma), the cells treated with different range of concentrations (6.25 μg/mL, 12.5 μg/mL, 25 μg/mL, 50 μg/mL, and 100 μg/mL) of AgNPs followed by incubation at 37 °C for 24 hr along with negative (medium with cells but without AgNPs) and positive control (Cisplatin 2.58 μg/mL, # PHR 1624 Sigma). The A549 cell lines were incubated with 0.5 mg/mL concentration of 3-(4, 5-dimethyl-2-thiazolyl)-2, 5-diphenyl tetrazolium bromide (MTT) at 37 °C for 3 hr. After 3 hr of incubation, media were aspirated slowly add 100 μL of dimethyl sulfoxide to each well to dissolve insoluble formazan crystals and incubated for 15 min. The percentage of cell viability calculated from the absorbance values recorded at 570 nm using an ELISA reader.

2.9. Anticancer activity by ROS (Reactive oxygen species) assay

In the ROS expression study, AgNPs were loaded at 10,000 cells/200 μL density in a 96-well plate and kept inside at 5% CO_2 incubation chamber at 24 hr at 37 °C. The used medium was aspirated and given a buffer wash with 100 μL of 1X phosphate buffer solution (PBS). The cells treated with H_2O_2 (100 μM) and test compounds with IC_{50} concentration were used except cell control and incubated for 24 hr. The 4 mM stock solution of dichloro di-hydro fluorescein di-acetate (H2DCFDA (Life Technologies Invitrogen, Catalog number: D-399) was diluted into Dulbecco's phosphate-buffered saline (D-PBS (# TL1006, Himedia)) to make 10 μM working solution freshly. The cells were stained with H2DCFDA working solution and kept for 2 hr at 37 °C in a dark chamber, the cell images are taken at different intervals of time (0–120 min) using a confocal microscope (Carl Zeiss, LSM 880) with excitation and emission wavelengths of 488 nm and 535 nm, respectively, for the FL1 (Fluorescence) channel and the fluorescent images were analyzed by Image J software and recorded. All the experiments conducted in triplicates in different time of intervals.

2.10. Preparation of SDS-PAGE and identification of AgNPs capping proteins

The proteins present on the surface of *Streptomyces hirsutus* strain SNPGA-8 silver nanoparticles were used for sodium dodecyl sulphate–polyacrylamide gel electrophoresis (SDS-PAGE) analysis as per Supriyo et al., (Chowdhury et al., 2014) with minor modifications in the protocol. Directly, about 50 μL of synthesized AgNPs supernatant was taken along with 50 μL of sample buffer (SDS) and mixed before boiling at 90 °C for 2 min. The wells were loaded with 15 μL of the prepared sample. Electrophoresis was performed in a 13% SDS-polyacrylamide gel using a Bio-Rad Mini-PROTEAN gel system at a constant voltage of 100 kV for 3 h. The post elec-

trophoresis gel was stained with Coomassie brilliant blue dye and observed in a gel-image.

3. Results

3.1. Green synthesis of AgNPs and UV–Vis. Analysis

Out of 45 Actinomycetes isolates, *Streptomyces hirsutus* strain SNPGA-8 was selected for the green synthesis of AgNPs. The AgNPs formation was observed by mixing the supernatant of *Streptomyces hirsutus* strain SNPGA-8 with 1 mM of silver nitrate solution in equal volumes. Adding supernatant to the reaction mixture changes the color from pale yellow to dark brown in about 120 hr (Fig. 1). The color change observed for the green synthesis of AgNPs samples was further confirmed by UV–Visible spectral scan (300–700 nm) as a part of primary confirmation. The strong characteristic absorption peak of the synthesized AgNPs was observed at 418 nm (Fig. 2). Broad peak absorption of UV data confirms the reduction of silver nitrate to silver nanoparticles by the culture supernatant of *Streptomyces hirsutus* strain SNPGA-8.

3.2. FTIR analysis

FT-IR analysis was carried out to obtain information about chemical groups present in the AgNPs for their stabilization and understand the transformation of functional groups due to the reduction process and FTIR scanning data obtained in the range of 4000–400 cm^{-1}. The spectrum showed several major and minor shifts of absorption bands at 3273, 2925, 1723, 1634, 1545, 1441, 1377, 1281, 1229, 1031, 979, 758, 496, 463, and 428 cm^{-1} indicating the presence of reduction and capping agents associated with AgNPs (Fig. 3). The intense band of 3273 cm^{-1} was a distinct group of O—H bonded alcohols, band at 2925 cm^{-1} corresponded to C—H stretching alkanes, 1723 cm^{-1} was identified as C=O aldehyde, 1634 cm^{-1} was correlated to C=C alkene. The peak at 1545 cm^{-1} attributed to C=C ring stretching alkene, peak at 1441 cm^{-1} assigned to the C—H bend of CH_2/CH_3 arene-ethylbenzene, the peak of 1377 cm^{-1} was correlated as C-X fluoride, the peak 1281 cm^{-1} corresponded to C—N amines. The peak at 1229 cm^{-1} was identified as S=O sulfones, sulfonyl chlorides, sulfates, sulfonamides, peak at 1031 cm^{-1} corresponds to C—N amines, and the peaks at 979 and 758 cm^{-1} were assigned to C—H out of plane bend alkenes and C-X chloride, respectively. The peaks at 496, 463, and 428 cm^{-1} are attributed to C-X bromide and iodide.

3.3. Thermo gravimetric analysis

The green synthesized silver nanoparticles were subjected to TGA analysis was used to assess the purity and thermal stability of capped silver nanoparticles, and data represented in the graph

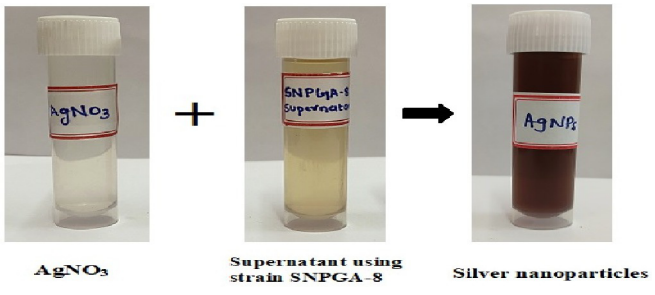

Fig. 1. Confirmation of the green synthesis of AgNPs; Colour changes in the *Streptomyces hirsutus* strain SNPGA-8 supernatant after addition of $AgNO_3$ for silver nanoparticles synthesis after 120 hr.

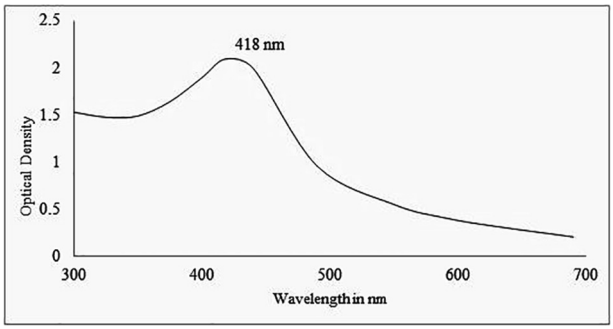

Fig. 2. UV–Vis. spectrum of *Streptomyces hirsutus* strain SNPGA-8, AgNPs.

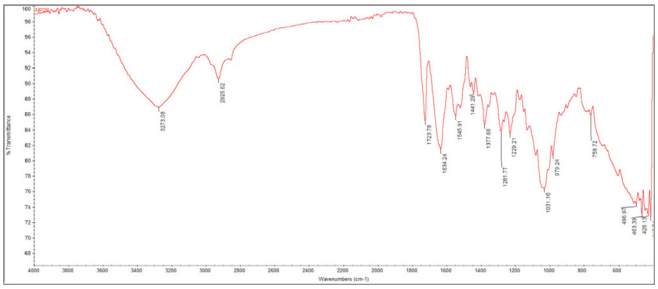

Fig. 3. FTIR spectrum of *Streptomyces hirsutus* strain SNPGA-8 AgNPs.

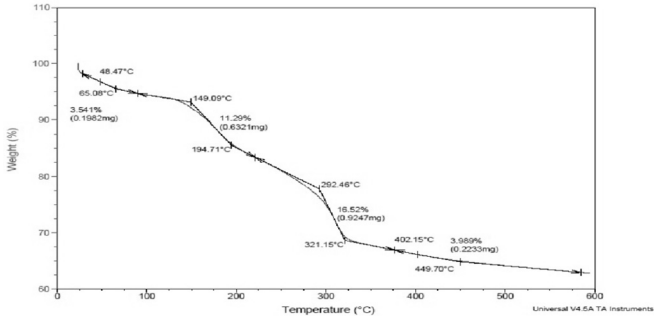

Fig. 4. Thermo gravimetric analysis of *Streptomyces hirsutus* strain SNPGA-8 AgNPs.

(weight (%) vs. temperature (°C)) has shown in Fig. 4. TGA observed multiple decompositions of the sample, and weight loss is may be due to the breaking of chemical bonds or interaction of chemicals with secondary metabolites of *Streptomyces hirsutus* strain SNPGA-8. The decomposition of the AgNPs was recorded at a constant rate of 10 °C/min. The core material, nitrogen, and oxygen are the main reason for the decomposition of the sample. Here we observed four phases of weight loss from room temperature to 600 °C. Initially, from room temperature to 150 °C, our sample shows good thermal stability with a weight loss of only 3.54%; this may be due to the evaporation of surface and interlayer water content present in living organisms and silver precursors. From the temperature above the 15 °C slowly, the weight loss increased with 11.29% up to 292 °C. This loss may be attributed to hydroxyl groups presence, breakdown of organic and inorganic elements present in the synthesis process. We observed a sudden decrease in the sample weight up to 321 °C, which is 16.52%. The precursors nitrates may reason for this, which may affect the crystal transformation or change in the shape of the crystal structure. In the last phase, from 321 °C to 600 °C, we did not observe any remarkable loss.

There we got only 3.98% of the loss. The thermal behavior of the synthesized Ag NPs shows good stability with a loss of around 35% from room temperature to 600 °C.

3.4. HR-TEM analysis

Further insight on morphology and size details of the bio-reduced AgNPs were determined using HR-TEM, and the data derived from *Streptomyces hirsutus* strain SNPGA-8 AgNPs. HR-TEM images of AgNPs revealed the formation of spherical in shape and poly-dispersed in nature. The particle size ranged from 18.99, 19.17, 21.95, 23.14, 25.00, 26.10, 29.18, 30.92, to 32.09 nm with the smallest particle size being 18.99 nm (Fig. 5).

3.5. SEM with EDX analysis

In Fig. 6A, scanning electron microscope (SEM) of surface imaging method that confirmed the nanomaterial shapes and size distribution. Using a SEM, the morphology of *Streptomyces hirsutus* strain SNPGA-8 synthesized AgNPs as spherical in shape and poly-dispersed were observed. EDX spectrometer analyses the abundance and distribution of specific elemental silver signals of the AgNPs. A trace elemental mapping of AgNPs by EDX pattern was obtained with C (48.82%), O (18.2%), Na (2.65%), Al (0.25%), Cl (5.25%), K (2.51%), and Ag (22.24%) as shown in Fig. 6B. A strong signal of the peak was observed at 3 keV and hinted the presence of silver in the synthesis of AgNPs sample.

3.6. XRD analysis

Powder XRD was done to know the structural information, phase purity, and crystalline nature of synthesized AgNPs. The four characteristic diffraction peaks were obtained at 38.11^0, 45.58^0, 64.62^0, and 77.51^0 and correlated to Braggs planes of (111), (200), (220) and (311) in XRD pattern (Fig. 7). The lattice plane values indicated the face-centered cubic (FCC) nature of AgNPs with a lattice parameter of a = 4.08 A0 and the average size of 12.74 nm for AgNPs.

3.7. Zeta potential analysis

Fig. 8 shows the zeta potential measurement of the stability of AgNPs was monitored spectroscopically by the zeta potential technique, which indicates the changes in the net surface charge with the time of the nanoparticles. The value of zeta potential single peak of AgNPs was obtained at −24.6 mV and suggested good stability and well-defined dispersion in the colloidal system.

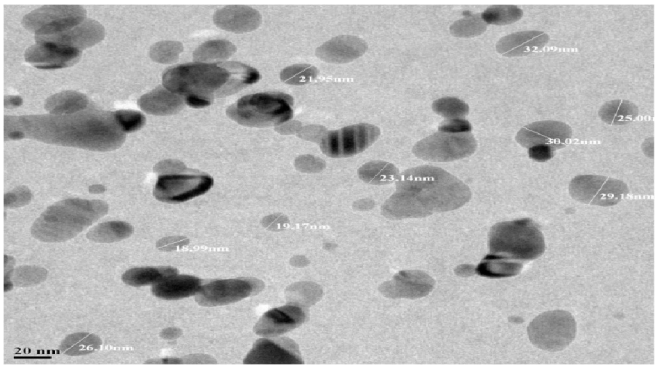

Fig. 5. HR-TEM micrograph of AgNPs.

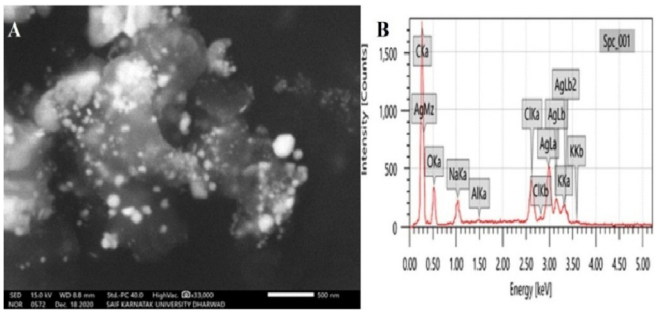

Fig. 6. SEM with EDX analysis of AgNPs synthesized with *Streptomyces hirsutus* strain SNPGA-8; (A) SEM micrograph image of AgNPs, (B) EDX spectrum showing elemental composition.

3.8. Genotypic characterization of a potent isolate

The most potent Actinomycete strain was identified by genotypic characterization analysis. The sequence of nucleotide 1096 base pairs obtained from the 16S rRNA gene of the *Streptomyces hirsutus* strain SNPGA-8 was submitted to the NCBI database of GenBank (Accession No. MW422853), the initially characterized by nucleotide BLAST to get homologous sequences. The phylogenetic tree was constructed by a relationship between representative experimental strains and the most closely related species as shown in Fig. 9.

3.9. Antimicrobial activity of AgNPs

The biosynthesized AgNPs displayed significant antimicrobial potential on selected pathogenic bacteria and fungi (Fig. 10A–H). The highest activity was recorded against *E. feacalis* and *S. aureus* with inhibition zones of 21 mm and 19 mm at a volume of 100 μL AgNPs suspension, respectively; with least activity was recorded against *P. aeruginosa* with 11, 12 and 13 and 12 mm inhibition zones at 25, 50, 75 and 100 μL of AgNPs suspension. At the same time, AgNPs showed moderate inhibition activity against the *E. coli* with 13, 15 and 16 and 17 mm. Similarly in the antifungal activity, the highest activity was found against *A. alternata* with an inhibition zone of 16, 17, 17, and 18 mm at volumes of at 25, 50, 75, and 100 μL AgNPs suspension. The least activity was recorded against *C. albicans* with 12, 13, 11, and 12 mm. At the same time, AgNPs showed moderate activity against the remaining two fungal pathogens like *F. oxysporum* and *C. glabrata* with 13, 14, 14, and 15 mm and 14, 15, 16, and 18 mm, respectively. The many research reports elucidated the possible modes of action for the antimicrobial mechanism by AgNPs; interestingly, the interaction with silver species with bacterial cell membrane damage, production of reactive oxygen species, enzyme inactivation, ribosome disassembly, protein denaturation, disruption of electron transport chain, and cell death occurs in pathogenic microbes, as illustrated in the possible mechanism (Fig. 11).

3.10. Minimum inhibitory concentration (MIC) and minimum bactericidal concentration (MBC)

In the study, the bacteriostatic activity of synthesized AgNPs towards *S. aureus*, *P. aeruginosa*, *E. faecalis*, and *E. coli* was studied. The MIC and MBC values of *Streptomyces hirsutus* strain SNPGA-8 AgNPs on pathogenic bacteria indicated the potential of AgNPs to inhibit bacterial cell growth even at the lowest concentrations of bacteriostatic activity. The AgNPs showed a considerable amount of microbial growth inhibition and the values of MIC and MBC were shown in Table 1.

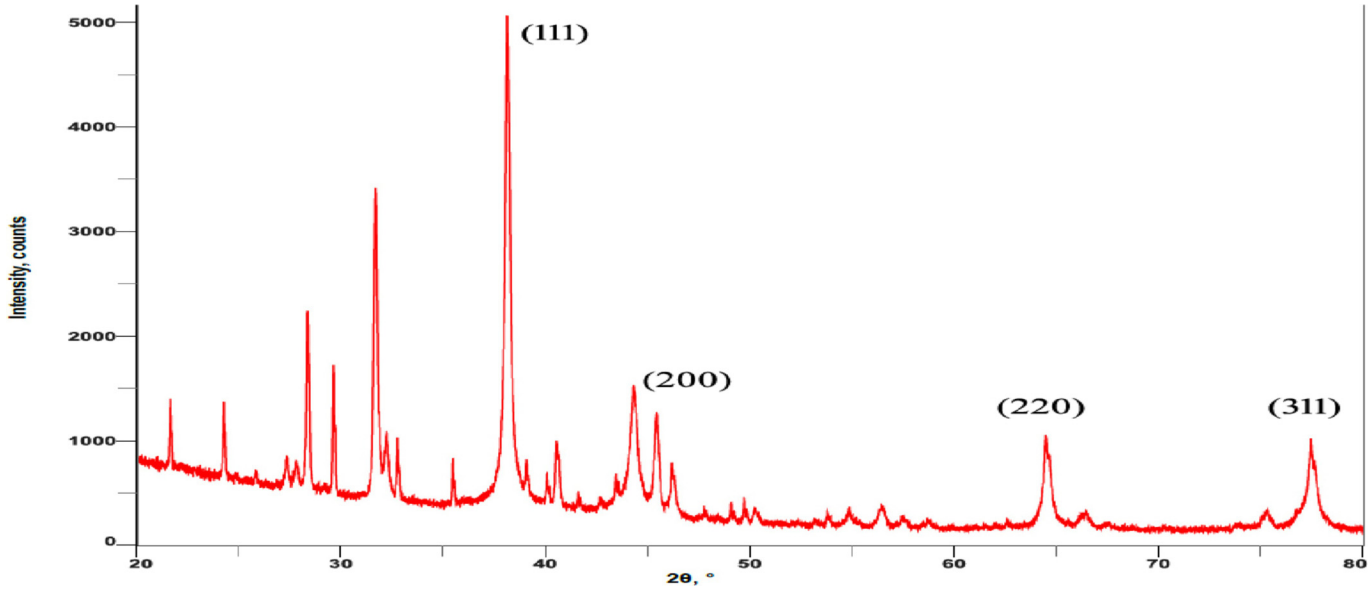

Fig. 7. XRD spectrum of AgNPs using strain SNPGA-8.

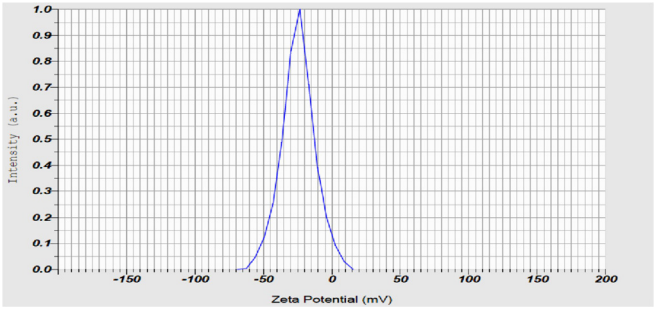

Fig. 8. Zeta potential of AgNPs synthesized with *Streptomyces hirsutus* strain SNPGA-8.

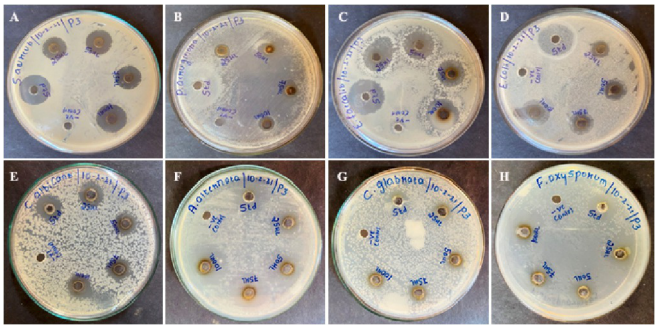

Fig. 10. Antimicrobial activity of *Streptomyces hirsutus* strain SNPGA-8; (A) *S. aureus*, (B) *P. aeruginosa*, (C) *E. faecalis*, (D) *E. coli*, (E) *C. albicans*, (F) *A. alternata*, (G) *C. glabrata* and (H) *F. oxysporum*.

Fig. 9. Phylogenetic tree analysis of *Streptomyces hirsutus* strain SNPGA-8.

3.11. Anticancer activity by MTT assay

The anticancer potential of synthesized silver nanoparticles using a supernatant of *Streptomyces hirsutus* strain SNPGA-8 against human lung carcinoma (A549) cell line. The A549 cell line exposed to AgNPs showed significant proliferation inhibition of the cell line. Morphological changes showed cell shrinkage and round at varying degree was visible in the images at dose different manner (6.25, 12.5, 25, 50, and 100 μg/mL) of AgNPs compared to negative and positive control were recorded using confocal microscopy, the results of cytotoxicity assay are represented in Fig. 12 A-G. In the present study, inhibited the cancer cells at a very low concentration at 6.25 μg/mL and 95% cell viability was observed significantly, when the more concentration of AgNPs (12.5, 25, 50, and 100 μg/mL), the cell viability was gradually decreased (75%, 57%, 35%, and 16%) as compared to negative and positive control (cisplatin at 46.27%). A potential AgNPs from *Streptomyces hirsutus* strain SNPGA-8 exhibited an IC_{50} value at 31.41 μg/mL by signifying a very strong cytotoxic activity against human lung cancer (A549) cell lines.

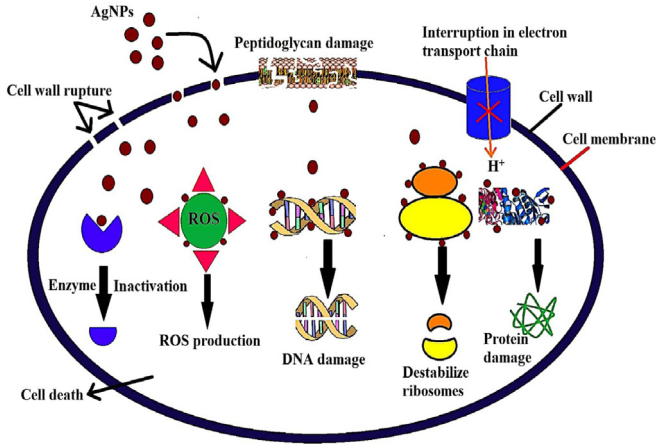

Fig. 11. A proposed model showing the possible mechanism of antimicrobial activity of AgNPs.

Table 1
MIC and MBC results of AgNPs synthesized by *Streptomyces hirsutus* strain SNPGA-8.

Sl. No.	Name of the Pathogen	MIC (μg/mL)	MBC (μg/mL)
1.	*S. aureus*	32	32
2.	*P. aeruginosa*	16	32
3.	*E. faecalis*	32	64
4.	*E. coli*	64	128

3.12. ROS (reactive oxygen species) assay

ROS generation measures the H2DCFDA expression in the A549 cell line by confocal microscopy at different intervals of times at IC_{50} (31.41 μg/mL) concentration of AgNPs. Reactive oxygen species are molecules containing hydroxyl radicals or peroxides with unpaired electrons. ROS are produced naturally as a byproduct of oxidative phosphorylation, oxidoreductase enzymes, or metal-catalyzed oxidation at a controlled rate in healthy aerobic cells. However, ROS can be induced under some stress conditions, especially exposure to environmental oxidants and specific drugs that lead to oxidative stress. Therefore, in this study, ROS expression determined by fluorescent dye (H2DCFDA) to detect the oxidation potential in A549 cells of morphology was observed in highly condensed, the formation of necrotic structure outside the cell membrane region completely damaged or ruptured, and immature cell colonies were observed. The intracellular ROS generation significantly increases at different time intervals in silver nanoparticles treated from human lung cancer (A549) cell line, as shown in Fig. 13A–G. In our study, the stronger fluorescent intensity of H2DCFDA dye was noticed and proved to inhibit the A549 cancer cell line. The increased ROS generation was due to increased treatment with different intervals of times at IC_{50} (31.41 μg/mL) concentration of AgNPs. As compared with control, as time increases, significantly increases in ROS generation observed in 120 min of AgNPs treated cells.

3.13. Analysis of AgNPs capping proteins with Streptomyces hirsutus strain SNPGA-8

In the present study, the extracellular AgNPs from *Streptomyces hirsutus* were characterized with SDS page analysis to determine protein surfaces that acted as capping agents (Fig. 14). SDS page revealed that in lane 2, illustrated AgNPs boiled with a buffer solution that showed an intense band for protein (44 kDa) associated with AgNPs as compared with reference molecular size marker (Fig. 14). The presence of protein at a molecular size of 44 kDa (Lane 2) as a capping or stabilizing agent in the AgNPs plays a vital role in the prevention of oxidation of elemental silver (Ag^0) into silver ions (Ag^+).

4. Discussion

With the recent advance in the field of AgNPs, many approaches were investigated by the synthesis of AgNPs from different plant parts like root, stem, fruits, leaf, flower buds and focus on microorganisms such as bacteria, fungi, Actinomycetes, and yeast. The synthesis of silver nanoparticles has a substantial impact on different applications in medicine, electronic, biomaterial, food, energy, gene delivery systems, nano-device fabrication, artificial implants, biosensing, drug delivery, and control plant pest disease in crops. Many scientific research areas investigate the synthesis of silver nanoparticles from Actinobacteria SL19, *Bacillus methylotrophic*,

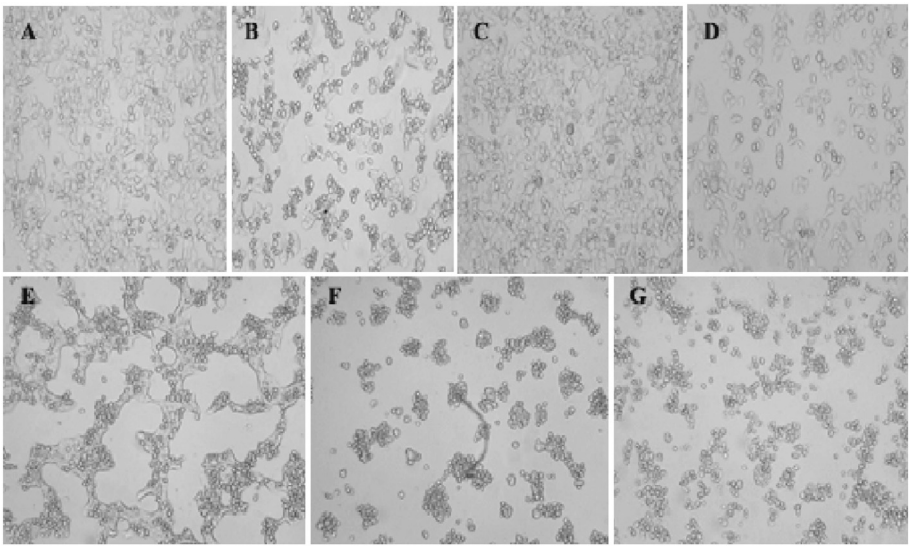

Fig. 12. Morphological changes in A549 cell line after exposure to different concentrations of AgNPs: (A) Negative control, (B) Positive control (cisplatin), (C) 6.25 μg/mL, (D) 12.5 μg/mL, (E) 25 μg/mL, (F) 50 μg/mL, and (G) 100 μg/mL of AgNPs.

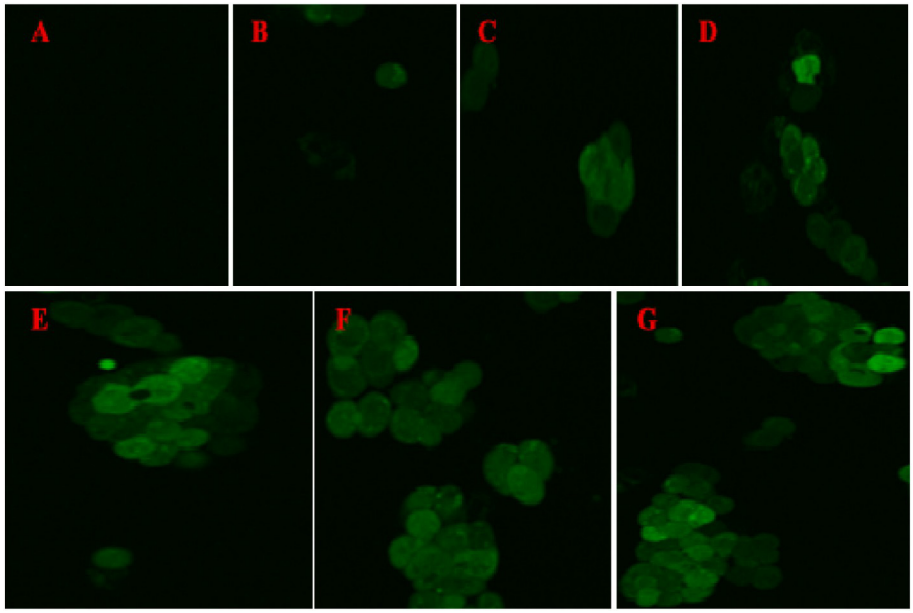

Fig. 13. ROS-mediated anticancer activity of *Streptomyces hirsutus* strain SNPGA-8 AgNPs on A549 cell line; (A) 0 min, (B) 5 min, (C) 15 min, (D) 30 min, (E) 60 min, (F) 90 min, and (G) 120 min of AgNPs treatment.

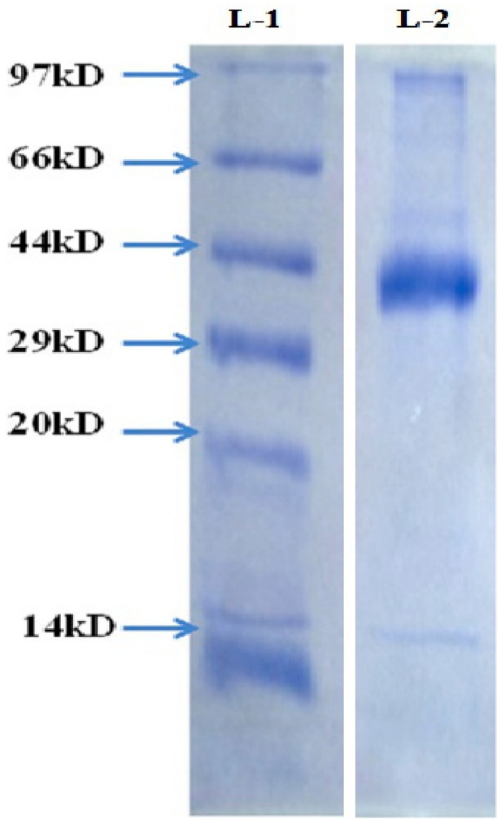

Fig. 14. SDS-PAGE analysis of proteins associated with AgNPs of *Streptomyces hirsutus* strain SNPGA-8; Lane-1 Molecular size marker, and Lane-2 Molecular size shows a major band 44 kDa.

Pseudomonas, and *Fusarium semitectum* cell-free supernatants (Ahmad et al., 2003; Alani et al., 2012; John et al., 2020; Wang et al., 2016). The present study reports the formation of biologically active Ag-NPs synthesized by *Streptomyces hirsutus* strain SNPGA-8. The synthesis of AgNPs reported, where the supernatant color changes after adding $AgNO_3$ were due to the formation of elemental silver (Ag^0) from the reduction of Ag^+ ions. Present study color change was observed where dark brown color was formed in the reaction mixture due to the reduction of elemental silver (Ag^0) from Ag^+ ions, and the excitation of strong peak of UV–visible data result confirms strong surface plasmon resonance (SPR) in the metal silver nanoparticles (Elamawi et al., 2018)

The FTIR spectrum showed several major and minor shifts in peak intensity of absorption bands involved in the various functional groups in biomolecules (See Fig. 3). These include alcohols, phenols, bromide, iodide, chlorides, and sulfates in the surface adsorption of functional groups. These are responsible for the bioreduction of silver and are associated with the reduction, stabilization, and capping of AgNPs (Elemike et al., 2017; Rodríguez-Luis et al., 2016). The TGA curve plot of the capped AgNPs of the sample are dominant weight loss occurred from room temperature at 600 °C temperature, and it shows as good thermal stability and only 3.54% weight loss observed, due to the evaporation of surface and interlayer water content present in living organisms and silver precursor. Similar findings were noticed by having close similarity to the adsorbed organic components and bioactive compounds attached to the surface of the silver nanoparticles (Chanthini et al., 2015; Sun et al., 2014). In general, different concentration of $AgNO_3$ gives stable nanoparticles, most of the synthesis of silver nanoparticles from various microorganisms are spherical in shapes ranging from 15 to 50 nm. The present study synthesis of silver nanoparticles TEM image ranging from 18 to 39 nm (See Fig. 5) and SEM image shows that the topography and morphology of AgNPs can be observed and calculate the size of AgNPs at micro and nanoscales. Based on the reported studies, it is clear that silver nanoparticles were obtained for higher pH (8.0); these are spherical in shape and homogeneous dispersion with particle sizes between 10 and 50 nm in different microorganisms (Salem et al., 2020; Menazea & Abdelghany, 2020). The working principle of EDX based on the collision of electrons with the nanoparticles to produce X-rays pattern of AgNPs was obtained with Ag and other atomic structure of each elemental composition present in the synthesized AgNPs from *Streptomyces* sp. A strong signal of the optical absorption peak was observed at 3 keV and hinted at the presence

of silver in the synthesis of AgNPs (Fouda et al., 2020). In the present study, four characteristics of silver diffraction peaks were obtained at Bragg's planes of (111), (200), (220), and (311) in XRD pattern (See Fig. 7). The lattice plane values indicated the face-centered cubic (FCC) nature of AgNPs with a lattice parameter of a = 4.08 A^0 and the average size of 12.74 nm for AgNPs. The same results reported by the synthesis of AgNPs are cubic, crystalline, and face-centered. A few unassigned peaks observed in the XRD pattern due to the presence of some proteins and bioorganic compounds in the *Streptomyces hirsutus* strain SNPGA-8 and crystallizes on the surface of the silver (Rodríguez-Luis et al., 2016). Zeta potential measures long-term stability was monitored, and control AgNPs with large positive/negative zeta potential repel each other (Elamawi et al., 2018). The zeta potential peak of AgNPs was obtained at −24.6 mV (See Fig. 8) and suggested good stability and well-defined dispersion in the colloidal system. The higher negative values indicated the higher stability and well-defined suspension of the synthesized AgNPs in the medium. The negative values confirmed the repulsion between the particles, which enhances the dispersity and stability of the synthesized AgNPs.

Based on the earlier reported studies, Actinomycetes nanoparticles have potent antimicrobial activity. The present study shows *Streptomyces hirsutus* strain SNPGA-8 synthesized AgNPs showed a reasonable zone of inhibition against *E. feacalis* and *S. aureus*, most miniature zone at *P. aeruginosa*, and moderate inhibition zone activity against the *E. coli*. This is because AgNPs, due to their killing activities against bacteria. Smaller sized AgNPs directly attached to bacteria's cell wall and quickly penetrate the bacterial cell wall and potentially disrupt the cellular components and ultimately cellular death. Similarly, the small size interaction of AgNPs is better with the targeted pathogen, and it is more effective. Similarly, the antifungal activity highest inhibition zone against *A. alternata*, least activity *C. albicans*, and moderate activity observed *F. oxysporum* and *C. glabrata*. Several reports have revealed that the antibacterial potential of AgNPs is more effective against gram-positive bacteria when compared with gram-negative bacteria because of their cell wall structure. And also, AgNPs with smaller diameters (1 to 20 nm) and size have increased stability, biocompatibility, and enhanced antimicrobial activity have proved against a wide range of fungi, bacteria, and viruses in a shape-dependent manner. The many research reports elucidated the possible modes of action for the antimicrobial mechanism by AgNPs (Al-Dhabi et al., 2019; Salem et al., 2020) The possible mechanism illustrated the specific activity of synthesized AgNPs and the synergistic effect of AgNP capping molecules against the studied bacteria (See Fig. 11). In this experiment, we determined the MIC is defined as the minimum concentration of antibiotic substance required to kill or inhibit the growth of bacteria, and MBC value was determined at which there was no visible bacterial growth. Meanwhile, MIC value might be lower to MBC, where there is less or no visible bacterial growth than the positive control. The equivalent and comparing observations were recorded in the earlier studies; the biosynthesized AgNPs manifested notable MIC and MBC values against pathogens by effectively hindering bacterial growth (Bhat et al., 2021).

The present study shows A549 cell line exposed to AgNPs showed significant proliferation inhibition of the cell line. Morphological changes showed cell shrinkage and rounding at varying degrees was visible in the images in a dose-dependent manner compared to a negative and positive control (See Fig. 12A–G). A notable decrease in cell viability when treated with a low concentration of AgNPs suggested that parameters like pH, nutrient, temperature, stress response, and a biochemical component may have contributed to the increased anticancer activity (Bhuvaneswari et al., 2017). Several studies reported the involvement of AgNPs surface in conjunction with the penetrative force of NPs well spread for the potent against cancerous cell lines such as human lung fibroblast (WI38) cell line, mammary gland breast cancer (MCF-7), human amnion (WISH) cell line, hepatocellular carcinoma (HepG-2) cell line, breast carcinoma (MCF-7) cell line, colon carcinoma (HCT-116) cell line, lung carcinoma (A-549) cell line, larynx carcinoma (HeP-2) cell line, intestinal carcinoma cell (CACO), prostate carcinoma (PC-3) cell line, and cervical carcinoma (HeLa) cell line (Abd-Elnaby et al., 2016; El-Naggar et al., 2018). The present study inhibited the cancer cells at a very low concentration at 6.25 μg/mL, and 95% cell viability was observed significantly decreases. Similar findings observed in a minimum concentration of AgNPs showed high activity against selected cancer cell lines. The spherical shape of AgNPs with different sizes ranging from 5 to 50 nm led to suitable inhibitory activities against the lymphoma Jurkat cell line with the IC_{50} value of 21.05 μg/mL (Salehi et al., 2016). Similar findings observed more cytotoxic effects on human lung epithelial (A549) cells. The probable reason was that the size and shape of the AgNPs directly contact the cell surfaces and initiate cytotoxicity (Gliga et al., 2014). The earlier studies indicated that Ag^o ions released from AgNPs have strong interaction with cells, the formation of membrane ruptures, DNA and RNA damage, breaks the lysosomal membrane; ATP gets reduced and inactive enzymes (Shukla et al., 2011). The present result was obtained from ROS generation in H2DCFDA expression in the A549 cell line. The fluorescent dye (H2DCFDA) to detect the oxidation potential in A549 cells of morphology was observed in highly condensed, and appearance of dissembled gaps between neighboring cells formation of necrotic structure and immature cell colonies are seen (See Fig. 13). The stronger fluorescent intensity was noticed due to increased treatment with different intervals of times at IC_{50} (31.41 μg/mL) concentration of AgNPs significantly increases in ROS generation inhibit the A549 cancer cell line at 120 min. Similar findings noticed in HepG-2 cells ROS generation at the concentration of 20 μg/mL play a vital role in the anticancer activity, and excess ROS generation can cause damage to the building blocks of cells, including DNA, proteins, and lipids, and eventually results in cell death (Bhakya et al., 2016; Gliga et al., 2014). In the present study, extracellular AgNPs were characterized with SDS page analysis to determine protein surfaces that acted as capping agents. The presence of protein at a molecular size of 44 kDa (Lane 2) as a capping or stabilizing agent in the AgNPs plays a vital role in the prevention of oxidation of elemental silver (Ag^o) into silver ions (Ag^+). A few studies reported that capping of protein expression of Actinomycetes synthesized AgNPs. A few bands were noted with a 20 and 30 kDa molecular weight by confirming proteins' presence in capping and stabilizing AgNPs (Sukanya et al., 2013). These results agreed with the earlier studies that protein associated with AgNPs observed in the SDS-PAGE at 85, 34, and 43 kDa acts as capping material and provides stability to the AgNPs (Chitra & Annadurai, 2013; Sukanya et al., 2013).

5. Conclusion

The present study reported a simple, eco-friendly green synthesis method of AgNPs by *Streptomyces hirsutus* strain SNPGA-8 extract. The AgNPs synthesis was primarily noted by the change in color of the reaction mixture and confirmed by absorption maximum at 418 nm in UV–Vis. analysis. The biomolecules associated with the reduction, stabilization, and capping of AgNPs were identified by IR bands in FTIR spectrum, and the morphological details of bio-reduced AgNPs were determined by using HR-TEM with an average size of 12.74 nm. The chemical composition of synthesized silver nanoparticles exhibited 22.24% Ag along with various other elements in EDX analysis. The biosynthesized AgNPs displayed significant antimicrobial activity on bacterial and fungal pathogens

with considerable MIC and MBC values. The cytotoxicity result suggested that *Streptomyces hirsutus* strain SNPGA-8 derived AgNPs significantly induced cell death in human lung carcinoma cells (A549). The increased ROS expression induced oxidative stress in cancer cells, which ultimately lead to apoptosis. AgNPs provide additional mechanical, optical, chemical, and biological peculiarities that recommend them for the design, obtaining, evaluation, and clinical assessment of performance-enhanced biomaterials and medical devices. Thus, the low toxicity, low production cost, and multiple potential possibilities of AgNPs for solving various biological problems make them prospective objects for the following scientific research and applications in the field of practical medicine.

Funding

This research was funded by the Deanship of Scientific Research of Princess Nourah bint Abdulrahman University through the Fast-track Research Funding Program.

Declaration of Competing Interest

The authors declare that they have no known competing financial interests or personal relationships that could have appeared to influence the work reported in this paper.

Acknowledgement

The authors would like to thank University Scientific Instrumentation Center (USIC), Karnatak University Dharwad, for extending instrumentation facilities. This research was funded by the Deanship of Scientific Research of Princess Nourah bint Abdulrahman University through the Fast-track Research Funding Program.

References

Abd-Elnaby, H., Abo-Elala, G., Abdel-Raouf, U., Abd-elwahab, A., Hamed, M., 2016. Antibacterial and anticancer activity of marine *Streptomyces parvus*: optimization and application. Biotechnol. Biotechnol. Equip. 30 (1), 180–191. https://doi.org/10.1080/13102818.2015.1086280.

Ahmad, A., Mukherjee, P., Senapati, S., Mandal, D., Khan, M.I., Kumar, R., Sastry, M., 2003. Extracellular biosynthesis of silver nanoparticles using the fungus *Fusarium oxysporum*. Colloids Surf. B 28 (4), 313–318. https://doi.org/10.1016/S0927-7765(02)00174-1.

Ahmed, R.H., Mustafa, D.E., 2020. Green synthesis of silver nanoparticles mediated by traditionally used medicinal plants in Sudan. Int. Nano Lett. 10 (1), 1–14. https://doi.org/10.1007/s40089-019-00291-9.

Al-Dhabi, N.A., Ghilan, A.-K., Esmail, G.A., Arasu, M.V., Duraipandiyan, V., Ponmurugan, K., 2019. Environmental friendly synthesis of silver nanomaterials from the promising *Streptomyces parvus* strain Al-Dhabi-91 recovered from the Saudi Arabian marine regions for antimicrobial and antioxidant properties. J. Photochem. Photobiol., B 197, 111529. https://doi.org/10.1016/j.jphotobiol.2019.111529.

Alani, F., Moo-Young, M., Anderson, W., 2012. Biosynthesis of silver nanoparticles by a new strain of *Streptomyces* sp. compared with *Aspergillus fumigatus*. World J. Microbiol. Biotechnol. 28 (3), 1081–1086. https://doi.org/10.1007/s11274-011-0906-0.

Avilala, J., Golla, N., 2019. Antibacterial and antiviral properties of silver nanoparticles synthesized by marine Actinomycetes. Int. J. Pharm. Sci. Res. 10 (3), 1223–1228.

Barai, A.C., Paul, K., Dey, A., Manna, S., Roy, S., Bag, B.G., Mukhopadhyay, C., 2018. Green synthesis of *Nerium oleander*-conjugated gold nanoparticles and study of its in vitro anticancer activity on MCF-7 cell lines and catalytic activity. Nano Converg. 5 (1), 10. https://doi.org/10.1186/s40580-018-0142-5.

Bhakya, S., Muthukrishnan, S., Sukumaran, M., Grijalva, M., Cumbal, L., Franklin Benjamin, J.H., Kumar, T.S., Rao, M.V., 2016. Antimicrobial, antioxidant and anticancer activity of biogenic silver nanoparticles- an experimental report. RSC Adv. 6 (84), 81436–81446. https://doi.org/10.1039/C6RA17569D.

Bhat, M., Chakraborty, B., Kumar, R.S., Almansour, A.I., Arumugam, N., Kotresha, D., Pallavi, S.S., Dhanyakumara, S.B., Shashiraj, K.N., Nayaka, S., 2021. Biogenic synthesis, characterization and antimicrobial activity of *Ixora brachypoda* (DC) leaf extract mediated silver nanoparticles. J. King Saud Univ. - Sci 33 (2), 101296. https://doi.org/10.1016/j.jksus.2020.101296.

Bhuvaneswari, R., Xavier, R.J., Arumugam, M., 2017. Facile synthesis of multifunctional silver nanoparticles using mangrove plant *Excoecaria agallocha* L. for its antibacterial, antioxidant and cytotoxic effects. J. Parasit. Dis. 41 (1), 180–187. https://doi.org/10.1007/s12639-016-0773-6.

Bray, F., Ferlay, J., Soerjomataram, I., Siegel, R.L., Torre, L.A., Jemal, A., 2018. Global cancer statistics 2018: GLOBOCAN estimates of incidence and mortality worldwide for 36 cancers in 185 countries. CA Cancer J. Clin. 68 (6), 394–424. https://doi.org/10.3322/caac.v68.610.3322/caac.21492.

Camas, M., Celik, F., Sazak Camas, A., Ozalp, H.B., 2019. Biosynthesis of gold nanoparticles using marine bacteria and Box-Behnken design optimization. Particulate Sci. Technol. 37 (1), 31–38. https://doi.org/10.1080/02726351.2017.1287794.

Chanthini, A.B., Balasubramani, G., Ramkumar, R., Sowmiya, R., Balakumaran, M.D., Kalaichelvan, P.T., Perumal, P., 2015. Structural characterization, antioxidant and in vitro cytotoxic properties of seagrass, Cymodocea serrulata (R.Br.) Asch. & & Magnus mediated silver nanoparticles. J. Photochem. Photobiol., B 153, 145–152. https://doi.org/10.1016/j.jphotobiol.2015.09.014.

Chitra, K., Annadurai, G., 2013. Bioengineered silver nanobowls using *Trichoderma viride* and its antibacterial activity against gram-positive and gram-negative bacteria. J. Nanostruct. Chem. 3 (1), 9. https://doi.org/10.1186/2193-8865-3-9.

Chowdhury, S., Basu, A., Kundu, S., 2014. Green synthesis of protein capped silver nanoparticles from phytopathogenic fungus *Macrophomina phaseolina* (Tassi) Goid with antimicrobial properties against multidrug-resistant bacteria. Nanoscale Res. Lett. 9 (1), 365. https://doi.org/10.1186/1556-276x-9-365.

Cory, A.H., Owen, T.C., Barltrop, J.A., Cory, J.G., 1991. Use of an aqueous soluble tetrazolium/formazan assay for cell growth assays in culture. Cancer Commun. 3 (7), 207–212. https://doi.org/10.3727/095535491820873191.

Culp, E.J., Yim, G., Waglechner, N., Wang, W., Pawlowski, A.C., Wright, G.D., 2019. Hidden antibiotics in Actinomycetes can be identified by inactivation of gene clusters for common antibiotics. Nat. Biotechnol. 37 (10), 1149–1154. https://doi.org/10.1038/s41587-019-0241-9.

Dahari, D.E., Mohamad Salleh, R., Mahmud, F., Lee, P.C., Embi, N., Mohd Sidek, H., 2016. Anti-malarial activities of two soil Actinomycete isolates from Sabah via inhibition of glycogen synthase kinase 3β. Trop. Life Sci. Res. 27 (2), 53–71. https://doi.org/10.21315/tlsr10.21315/tlsr2016.27.210.21315/tlsr2016.27.2.5.

Dholakiya, R.N., Kumar, R., Mishra, A., Mody, K.H., Jha, B., 2017. Antibacterial and antioxidant activities of novel Actinobacteria strain isolated from Gulf of Khambhat, Gujarat. Front. Microbiol. 8 (2420). https://doi.org/10.3389/fmicb.2017.02420.

Eisa, N.E., Almansour, S., Alnaim, I.A., Ali, A.M., Algrafy, E., Ortashi, K.M., Awad, M.A., Virk, P., Hendi, A.A., Eissa, F.Z., 2020. Eco-synthesis and characterization of titanium nanoparticles: testing its cytotoxicity and antibacterial effects. Green Process. Synth. 9 (1), 462–468. https://doi.org/10.1515/gps-2020-0045.

El-Naggar, N.E., Hussein, M.H., El-Sawah, A.A., 2018. Phycobiliprotein-mediated synthesis of biogenic silver nanoparticles, characterization, in vitro and in vivo assessment of anticancer activities. Sci. Rep. 8 (1), 8925. https://doi.org/10.1038/s41598-018-27276-6.

Elamawi, R.M., Al-Harbi, R.E., Hendi, A.A., 2018. Biosynthesis and characterization of silver nanoparticles using *Trichoderma longibrachiatum* and their effect on phytopathogenic fungi. Egypt. J. Biol. Pest Control. 28 (1), 28. https://doi.org/10.1186/s41938-018-0028-1.

Elemike, E.E., Fayemi, O.E., Ekennia, A.C., Onwudiwe, D.C., Ebenso, E.E., 2017. Silver nanoparticles mediated by *Costus afer* leaf extract: synthesis, antibacterial, antioxidant and electrochemical properties. Mol. 22 (5), 701.

Fouda, A., Hassan, S.-E.-D., Abdo, A.M., El-Gamal, M.S., 2020. Antimicrobial, antioxidant and larvicidal activities of spherical silver nanoparticles synthesized by Endophytic *Streptomyces* spp. Biol. Trace Elem. Res. 195 (2), 707–724. https://doi.org/10.1007/s12011-019-01883-4.

Gliga, A.R., Skoglund, S., Odnevall Wallinder, I., Fadeel, B., Karlsson, H.L., 2014. Size-dependent cytotoxicity of silver nanoparticles in human lung cells: the role of cellular uptake, agglomeration and Ag release. Particle Fibre Toxicol. 11 (1), 11. https://doi.org/10.1186/1743-8977-11-11.

Hamed, A.A., Kabary, H., Khedr, M., Emam, A.N., 2020. Antibiofilm, antimicrobial and cytotoxic activity of extracellular green-synthesized silver nanoparticles by two marine-derived Actinomycete. RSC Adv. 10 (17), 10361–10367. https://doi.org/10.1039/C9RA11021F.

Hassan, S.E., Fouda, A., Radwan, A.A., Salem, S.S., Barghoth, M.G., Awad, M.A., Abdo, A.M., El-Gamal, M.S., 2019. Endophytic Actinomycetes *Streptomyces* spp mediated biosynthesis of copper oxide nanoparticles as a promising tool for biotechnological applications. J. Biol. Inorg. Chem. 24 (3), 377–393. https://doi.org/10.1007/s00775-019-01654-5.

Imani, M.M., Safaei, M., 2019. Optimized synthesis of magnesium oxide nanoparticles as bactericidal agents. J. Nanotechnol. 2019, 1–6. https://doi.org/10.1155/2019/6063832.

John, M.S., Nagoth, J.A., Ramasamy, K.P., Mancini, A., Giuli, G., Natalello, A., Ballarini, P., Miceli, C., Pucciarelli, S., 2020. Synthesis of bioactive silver nanoparticles by a *Pseudomonas* strain associated with the Antarctic psychrophilic protozoon *Euplotes focardii*.. Mar. Drugs 18 (1), 38. https://doi.org/10.3390/md18010038.

Kalpana, V.N., Kataru, B.A.S., Sravani, N., Vigneshwari, T., Panneerselvam, A., Devi Rajeswari, V., 2018. Biosynthesis of zinc oxide nanoparticles using culture filtrates of *Aspergillus niger*: Antimicrobial textiles and dye degradation studies. Open Nano. 3, 48–55. https://doi.org/10.1016/j.onano.2018.06.001.

Kumari, S., Tehri, N., Gahlaut, A., Hooda, V., 2020. Actinomycetes mediated synthesis, characterization, and applications of metallic nanoparticles. Inorg. Nano-Metal. Chem. 1–10. https://doi.org/10.1080/24701556.2020.1835978.

Lee, S.H., Jun, B.H., 2019. Silver nanoparticles: synthesis and application for nanomedicine. Int. J. Molecular Sci. 20 (4), 865.
Ma, J., Cao, B., Liu, C., Guan, P., Mu, Y., Jiang, Y., Han, L., Huang, X., 2018. Actinofuranones D-I from a lichen-associated Actinomycetes, *Streptomyces gramineus*, and their anti-inflammatory effects. Mol. 23 (9), 2393.
Manivasagan, P., Venkatesan, J., Sivakumar, K., Kim, S.K., 2014. Pharmaceutically active secondary metabolites of marine Actinobacteria. Microbiol. Res. 169 (4), 262–278. https://doi.org/10.1016/j.micres.2013.07.014.
Menazea, A.A., Abdelghany, A.M., 2020. Precipitation of silver nanoparticle within silicate glassy matrix via Nd: YAG laser for biomedical applications. Radiat. Phys. Chem. 174, 108958.
Menazea, A.A., Awwad, N.S., 2020. Antibacterial activity of TiO_2 doped ZnO composite synthesized via laser ablation route for antimicrobial application. J. Mater. Res. Technol. 9 (4), 9434–9441.
Mikhailova, E.O., 2020. Silver nanoparticles: mechanism of action and probable bio-application. J. Funct. Biomater. 11 (4), 84.
Nayaka, S., Chakraborty, B., Bhat, M.P., Nagaraja, S.K., Airodagi, D., Swamy, P.S., Rudrappa, M., Hiremath, H., Basavarajappa, D.S., Kanakannanavar, B., 2020a. Biosynthesis, characterization, and in vitro assessment on cytotoxicity of Actinomycete-synthesized silver nanoparticles on *Allium cepa* root tip cells. Beni-Suef Univ. J. Basic Appl. Sci. 9 (1), 51. https://doi.org/10.1186/s43088-020-00074-8.
Nayaka, S.R., Chakraborty, B.I., Pallavi, S.S., Bhat, M.P., Shashiraj, K.N., Ghasti, B.H., 2020b. Synthesis of biogenic silver nanoparticles using Zanthoxylum rhetsa (Roxb.) DC seed coat extract as reducing agent and in-vitro assessment of anticancer effect on A549 lung cancer cell line. Int. J. Pharm. Res. 12, 304–314.
Ratnakomala, S., Fahrurrozi, Yopi, 2019. Enhancement of Cellulase (CMCase) production from marine Actinomycetes Streptomyces sp. Bse 7-9: Optimization of fermentation medium by Response Surface Methodology. In: Presented at the IOP Conference Series: Earth Environ. Sci.
Rodríguez-Luis, Osvelia E., Hernandez-Delgadillo, Rene, Sánchez-Nájera, Rosa Isela, Martínez-Castañón, Gabriel Alejandro, Niño-Martínez, Nereyda, Sánchez Navarro, María del Carmen, Ruiz, Facundo, Cabral-Romero, Claudio, 2016. Green synthesis of silver nanoparticles and their bactericidal and antimycotic activities against oral microbes. J. Nanomater. 2016, 1–10. https://doi.org/10.1155/2016/9204573.
Salem, Salem S., EL-Belely, Ehab F., Niedbała, Gniewko, Alnoman, Maryam M., Hassan, Saad El-Din, Eid, Ahmed Mohamed, Shaheen, Tharwat I., Elkelish, Amr, Fouda, Amr, 2020. Bactericidal and in-vitro cytotoxic efficacy of silver nanoparticles (Ag-NPs) fabricated by endophytic actinomycetes and their use as coating for the textile fabrics. Nanomater 10 (10), 2082. https://doi.org/10.3390/nano10102082.
Salem, S.S., Fouda, A., 2021. Green synthesis of metallic nanoparticles and their prospective biotechnological applications: an overview. Biol. Trace Elem. Res. 199 (1), 344–370. https://doi.org/10.1007/s12011-020-02138-3.
Salehi, S., Shandiz, S.A., Ghanbar, F., Darvish, M.R., Ardestani, M.S., Mirzaie, A., Jafari, M., 2016. Phytosynthesis of silver nanoparticles using Artemisia marschalliana Sprengel aerial part extract and assessment of their antioxidant, anticancer, and antibacterial properties. Int J Nanomed. 29 (11), 1835-46. https://doi.org/10.2147/IJN.S99882.
Saravanakumar, K., Chelliah, R., MubarakAli, D., Oh, D.H., Kathiresan, K., Wang, M.H., 2019. Unveiling the potentials of biocompatible silver nanoparticles on human lung carcinoma A549 cells and *Helicobacter pylori*.. Sci. Rep. 9 (1), 5787. https://doi.org/10.1038/s41598-019-42112-1.
Shukla, R.K., Sharma, V., Pandey, A.K., Singh, S., Sultana, S., Dhawan, A., 2011. ROS-mediated genotoxicity induced by titanium dioxide nanoparticles in human epidermal cells. Toxicol. In Vitro 25 (1), 231–241. https://doi.org/10.1016/j.tiv.2010.11.008.
Sukanya, M.K., Saju, K.A., Praseetha, P.K., Sakthivel, G., 2013. Therapeutic potential of biologically reduced silver nanoparticles from Actinomycete cultures. J. Nanosci. 2013, 1–8. https://doi.org/10.1155/2013/940719.
Sun, Q., Cai, X., Li, J., Zheng, M., Chen, Z., Yu, C.-P., 2014. Green synthesis of silver nanoparticles using tea leaf extract and evaluation of their stability and antibacterial activity. Colloids Surf. A 444, 226–231. https://doi.org/10.1016/j.colsurfa.2013.12.065.
Sung, Y.K., Kim, S.W., 2019. Recent advances in the development of gene delivery systems. Biomater. Res. 23 (1), 8. https://doi.org/10.1186/s40824-019-0156-z.
Tian, S., Saravanan, K., Mothana, R.A., Ramachandran, G., Rajivgandhi, G., Manoharan, N., 2020. Anti-cancer activity of biosynthesized silver nanoparticles using *Avicennia marina* against A549 lung cancer cells through ROS/mitochondrial damages. Saudi J. Biol. Sci. 27 (11), 3018–3024. https://doi.org/10.1016/j.sjbs.2020.08.029.
Vijayabharathi, R., Sathya, A., Gopalakrishnan, S., 2018. Extracellular biosynthesis of silver nanoparticles using *Streptomyces griseoplanus* SAI-25 and its antifungal activity against *Macrophomina phaseolina*, the charcoal rot pathogen of sorghum. Biocatalyst. Agri. Biotechnol. 14, 166–171. https://doi.org/10.1016/j.bcab.2018.03.006.
Wang, C., Kim, Y.J., Singh, P., Mathiyalagan, R., Jin, Y., Yang, D.C., 2016. Green synthesis of silver nanoparticles by *Bacillus methylotrophicus* and their antimicrobial activity. Artif. Cells Nanomed. Biotechnol. 44 (4), 1127–1132. https://doi.org/10.3109/21691401.2015.1011805.
Wolny-Koładka, K.A., Malina, D.K., 2018. Eco-friendly approach to the synthesis of silver nanoparticles and their antibacterial activity against *Staphylococcus* spp. and *Escherichia coli*. J. Environ. Sci. Health A. 53 (12), 1041–1047. https://doi.org/10.1080/10934529.2018.1474568.
Wypij, M., Czarnecka, J., Swiecimska, M., Dahm, H., Rai, M., Golinska, P., 2018. Synthesis, characterization and evaluation of antimicrobial and cytotoxic activities of biogenic silver nanoparticles synthesized from *Streptomyces xinghaiensis* OF1 strain. World J. Microbiol. Biotechnol. 34 (2), 23. https://doi.org/10.1007/s11274-017-2406-3.
Zahin, N., Anwar, R., Tewari, D., Kabir, M.T., Sajid, A., Mathew, B., Uddin, M.S., Aleya, L., Abdel-Daim, M.M., 2020. Nanoparticles and its biomedical applications in health and diseases: special focus on drug delivery. Environ. Sci. Pollut. Res. Int. 27 (16), 19151–19168. https://doi.org/10.1007/s11356-019-05211-0.
Zhang, H., Zhang, S., Peng, Y., Li, Y., Chen, Z., Xu, H., Yu, Z., Zheng, W., Zheng, T., 2015. Effects of marine Actinomycete on the removal of a toxicity alga *Phaeocystis globose* in eutrophication waters. Front. Microbiol. 6 (474). https://doi.org/10.3389/fmicb.2015.00474.
Ziąbka, Magdalena, Menaszek, Elżbieta, Tarasiuk, Jacek, Wroński, Sebastian, 2018. Biocompatible nanocomposite implant with silver nanoparticles for Otology-in-vivo evaluation. Nanomater. 8 (10), 764. https://doi.org/10.3390/nano8100764.